LAWRENCE
LIVERMORE
NATIONAL
LABORATORY

LLNL-JRNL-417591

Photoionized Features in the X-ray Spectrum of EX Hydrae

G. J. M. Luna, J. C. Raymond, N. S. Brickhouse, C. W. Mauche, D. Proga, D. Steeghs, R. Hoogerwerf

October 6, 2009

Astrophysical Journal

Disclaimer

Photoionized features in the X-ray spectrum of EX Hydrae

G. J. M. Luna[1], J. C. Raymond[1], N. S. Brickhouse[1], C. W. Mauche[2], D. Proga[3], D. Steeghs[4], R. Hoogerwerf[5]

Received _____; accepted _____

[1]Harvard-Smithsonian Center for Astrophysics, 60 Garden St., Cambridge, MA, 02138, USA.

[2]Lawrence Livermore National Laboratory, L-473, 7000 East Avenue, Livermore, CA 94550, USA

[3]Department of Physics and Astronomy, University of Nevada, 4505 South Maryland Parkway, Box 454002, Las Vegas, NV, 89154-4002, USA.

[4]Department of Physics, University of Warwick, Coventry CV4 7AL, UK.

[5]Interactive Supercomputing, Inc., 135 Beaver Street, Waltham, MA 02452, USA.

ABSTRACT

We present the first results from a long (496 ks) *Chandra* High Energy Transmission Grating observation of the intermediate polar EX Hydrae. In addition to the narrow emission lines from the cooling post-shock gas, for the first time we have detected a broad component in some of the X-ray emission lines, namely O VIII λ18.97, Mg XII λ8.42, Si XIV λ6.18, and Fe XVII λ16.78. The broad and narrow components have widths of $\sim$ 1600 km s^{-1} and $\sim$ 150 km s^{-1}, respectively. We also find that the flux of the broad component is modulated at the white dwarf spin period, constraining the region where the gas is formed. We propose a scenario where the broad component is formed in the pre-shock flow photoionized by radiation from the post-shock flow. Because the photoionized region has to be close to the radiation source in order to produce strong photoionized emission lines from ions like O VIII, Mg XII, and Si XIV, our photoionization model constrains the height of the standing shock above the white dwarf surface.

Subject headings: Binaries: cataclysmic variables — stars: individual (EX Hydrae) — intermediate polar — X-rays: binaries

1. Introduction

EX Hydrae (EX Hya) belongs to a sub-class of magnetic cataclysmic variables (CVs), known as intermediate polars (IPs), wherein the white dwarf (WD) magnetic field (≈ 0.2 MG) channels the accreting material from the inner edge of the truncated accretion disk through the accretion curtains and accretion columns to spots near the magnetic poles (Rosen et al. 1988). In this model, the magnetically channeled material reaches highly supersonic velocities in the pre-shock flow ($v_{\rm ff} = [2GM_{\rm WD}/R_{\rm WD}]^{1/2} = 6000$ km s^{-1}, where $v_{\rm ff}$ is the free-fall velocity for a WD of mass $M_{\rm WD} = 0.79\ M_{\odot}$ and radius $R_{\rm WD} = 5.9 \times 10^8$ cm) before passing through a strong stand-off shock near the WD surface, where nine-sixteenths of its kinetic energy is converted into thermal energy, heating the gas to temperatures of ~ 20 keV (Fujimoto & Ishida 1987; Brunschweiger et al. 2009). Below the shock, in the post-shock flow, the cooling material radiates its thermal and residual gravitational energy through free-free, bound-bound, and free-bound radiation, which is primarily detected in X-rays.

The nature of the observed X-ray spectrum of CVs depends primarily on the specific accretion rate (i.e., the accretion rate per unit area). The small spot size and hence high specific accretion rate of magnetic CVs impose a conical geometry that does not allow the X-ray photons to escape without further interaction, thus the observed X-ray spectrum is dominated by emission lines formed in a region photoionized by the radiation field from the shocked region. On the other hand, the boundary layer at the inner edge of the accretion disk of non-magnetic CVs covers a relatively large area and therefore the specific accretion rate is low, allowing the X-ray photons to escape freely. Mukai et al. (2003) observed this "binomial" distribution in moderately exposed (~ 100 ks) observations obtained with *Chandra* using the High Energy Transmission Grating (HETG), and found that the X-ray spectra of magnetic CVs are compatible with photoionized emission while

those of non-magnetic CVs are consistent with a collisionally ionized, cooling gas (known as a cooling-flow model in X-ray spectra fitting packages such as XSPEC[1]). Interestingly, EX Hya was the "exception" in this binomial distribution: its X-ray spectrum was well fit with a cooling-flow model. This can be explained if EX Hya has a tall, lower density shock (Allan et al. 1998), a lower accretion rate, and/or larger accretion spots than other IPs, and therefore a low specific accretion rate, leading to a dominant collisionally ionized, cooling spectrum.

Overall, the details of the temperature and density distribution in the post-shock flow are not yet well understood. In their analysis of a $\sim$ 60 ks *Chandra* HETG observation, Hoogerwerf et al. (2006) found spikes on both sides of the maximum of the light curve of He-like Mg XI emission line. These spikes appear at the exact moment of the WD spin cycle when the two accretion columns are visible on the limbs of the WD. In contrast to what is expected from simple cooling models, no spikes were present in the H-like Mg XII light curve, suggesting discrepancies with the standard cooling picture proposed by Aizu (1973).

We have obtained a deeper observation of EX Hya with the *Chandra* HETG in order to study a number of accretion-related phenomena. In this Letter, we present new results from this observation discussed in § 2. In § 3 we present an analysis of the X-ray line profiles that require a broad component, and a photoionization model to explain it. Discussion and conclusions are presented in § 4.

2. Observations

EX Hya was observed with *Chandra* using the HETG in combination with the ACIS-S for 496 ks. The observation was obtained in four segments (ObsIDs 7449: start time 2007

[1]http://heasarc.gsfc.nasa.gov/docs/xanadu/xspec/

May 13 22:15:35 UT, exposure time 130.65 ks; 7452: start time 2007 May 17 03:12:38 UT, exposure time 49.17 ks, 7450: start time 2007 May 18 21:56:57 UT, exposure time 162.73 ks; and 7451: start time 2007 May 21 14:15:08 UT, exposure time 153.07 ks). We extracted High Energy Grating (HEG) and Medium Energy Grating (MEG) ± first-order spectra and Ancillary Responce Matrices (ARFs) using the CIAO[2] script `fullgarf`, while Response Matrix Functions (RMFs) were extracted using `mkgrmf` script. We then combined ARFs and spectra from each observation segment using the `add_grating_spectra` script.

3. Emission line profiles

3.1. Line profiles analysis

In order to test models of the cooling of the post-shock gas, we attempted to measured the fluxes of the strong emission lines observed in the *Chandra* HETG spectrum using a model consisting of a Gaussian to represent the emission line and a first-order polynomial to represent the nearby continuum. We found that some of the strong emission lines were poorly fit with such a model, and that acceptable fits to these lines, in particular O VIII λ18.97, Mg XII λ8.42, Si XIV λ6.18, and Fe XVII λ16.78, could be obtained by adding a second Gaussian to represent the broad line wings. All the fit parameters were free to vary and their confidence limits determined to 90% confidence. Figure 1 shows the studied emission lines together with the best-fit models. Central wavelength, Full Width Half Maximum (FWHM), and observed flux of the narrow and broad components of each line are listed in Table 1.

An instrumental origin for these broad emission lines seems unlikely. The broad component is detected in four spectral orders simultaneously (HEG and MEG ±1), whereas

[2] *Chandra* Interactive Analysis of Observations (CIAO v. 4.1)

any broadening in the dispersion direction of a diffraction arm should not affect the dispersion in the other arm. Moreover, similarly deeply exposed observations (e.g., TW Hya, exposure time: 489 ks) with the same instrumental configuration as our observation of EX Hya do not show similar broad features (N. S. Brickhouse, personal communication).

3.2. Variability of the broad component

The narrow components of the emission lines formed in the region where the gas is cooling to settle down onto the WD are known to be modulated at the spin period of the WD (e.g., Allan et al. 1998; Hoogerwerf et al. 2006). Also, broad-band spectral fits show that the intervening absorption column, $N_{\rm H}$, is modulated at the spin period (Allan et al. 1998).

We constructed light curves folded at the WD spin period (assuming the ephemeris of Mauche et al. 2009) by extracting photons from the red and blue sides of the broad component of O VIII. We considered the broad profile to extend $\pm 4\,\sigma_{\rm broad}$ from the central wavelength $\lambda_{\rm broad}$ and subtracted the narrow profile which covers the $\lambda_{\rm narrow} \pm 4\,\sigma_{\rm narrow}$ wavelength range (see Table 1). Figure 2 shows the extracted light curves and fits with a sine function $A + B\,\sin 2\pi(\phi - \phi_0)$ with $A = 0.00018 \pm 0.00001$, $B = 0.00007 \pm 0.00001$, and $\phi_0 = 0.22 \pm 0.02$ for the flux on the blue side of the line and $A = 0.00017 \pm 0.00001$, $B = 0.00011 \pm 0.00001$, and $\phi_0 = 0.22 \pm 0.01$ for the flux on the red side of the line. Both sides of the broad component are clearly modulated at the spin period, with pulse fractions $B/A = 0.38 \pm 0.05$ and $B/A = 0.64 \pm 0.05$ for the blue and red sides of the line, respectively. [Please check my math on the ratios and errors. Why are the pulse amplitudes so different?]

Table 1. Line Fit Parameters [Do you like what I've done with this table?][J: Ohh, yes, thanks, much better]

	Narrow Component			Broad Component		
Line[a]	λ[b] (Å)	FWHM[c] (km s^{-1})	Flux[d]	λ[b] (Å)	FWHM[c] (km s^{-1})	Flux[d]
O VIII λ18.97	$18.972^{+0.006}_{-0.006}$	315^{+34}_{-25}	$7.13^{+0.4}_{-0.3}$	$18.972^{+0.011}_{-0.011}$	1922^{+230}_{-162}	$2.77^{+0.3}_{-0.3}$
Mg XII λ8.42	$8.424^{+0.006}_{-0.006}$	360^{+41}_{-34}	$1.08^{+0.09}_{-0.08}$	$8.422^{+0.006}_{-0.006}$	1329^{+176}_{-108}	$0.53^{+0.10}_{-0.09}$
Si XIV λ6.18	$6.183^{+0.006}_{-0.006}$	410^{+23}_{-57}	$1.09^{+0.03}_{-0.10}$	$6.185^{+0.006}_{-0.006}$	1297^{+69}_{-78}	$0.84^{+0.03}_{-0.05}$
Fe XVII λ16.78	$16.777^{+0.024}_{-0.012}$	117^{+42}_{-50}	$2.75^{+0.18}_{-0.15}$	$16.783^{+0.019}_{-0.018}$	1963^{+1247}_{-511}	$0.55^{+0.19}_{-0.21}$

[a]O VIII and Fe XVII were fit using only the MEG arm; Si XIV and Mg XII were fit using both the HEG and MEG arms.

[b]Absolute wavelength accuracy: HEG = 0.006 Å, MEG = 0.011 Å. Relative wavelength accuracy: HEG = 0.0010 Å, MEG = 0.0020 Å (*Chandra* Proposer's Observatory Guide v11.0)

[c]FWHM $\approx 2.3548\sigma$.

[d]Units of 10^{-4} photons cm^{-2} s^{-1}.

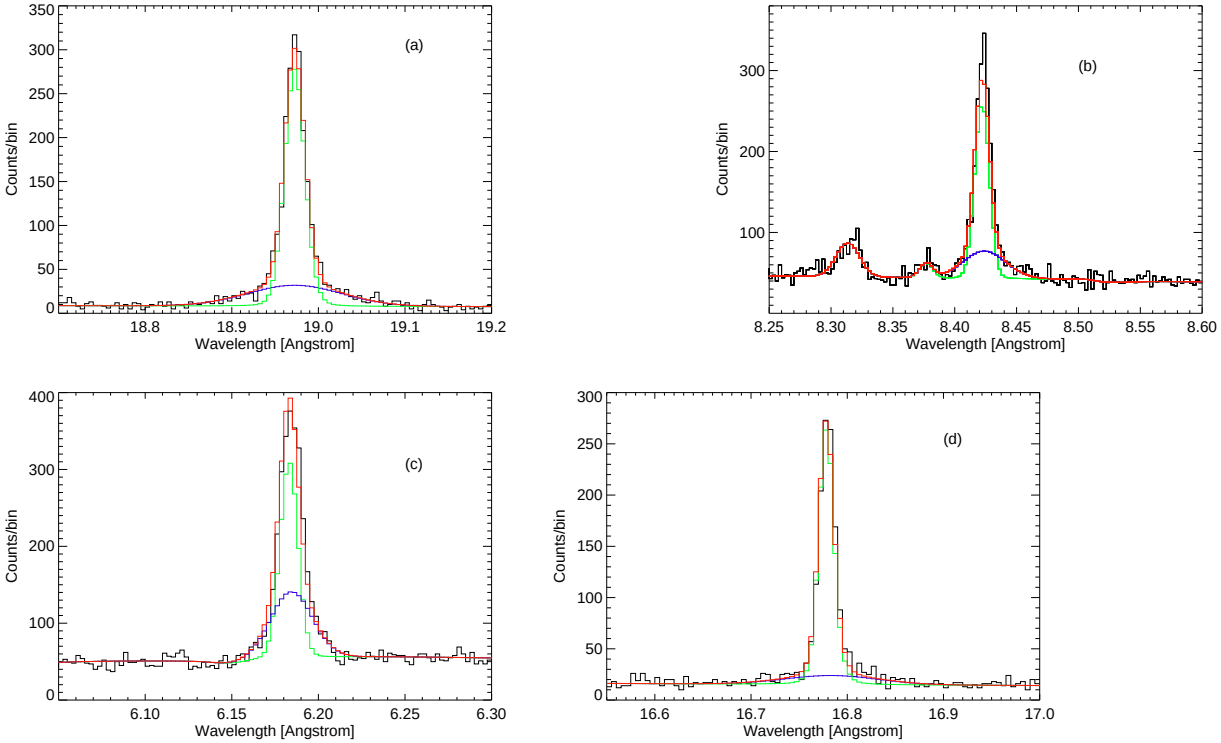

Fig. 1.— Observed emission line profiles with overlaid 2-Gaussian models of (*a*) O VIII λ18.97 (MEG −1), (*b*) Mg XII λ8.42 (HEG −1), (*c*) Si XIV λ6.18 (HEG −1), and (*d*) Fe XVII λ16.78 (MEG −1). Data are shown by the black histograms and the narrow, broad, and net model profiles are shown by the green, blue, and red histograms, respectively. The two emission lines (Fe XXI–XXIV λ8.31 and Fe XXIV λ8.38) in the vicinity of Mg XII λ8.42 were also included in the fit.

3.3. The photoionization model

Of the three regions of the magnetically controlled accretion flow — the accretion curtains, where the flow rises up and away from the truncated accretion disk; the pre-shock flow, where the relatively cool flow falls with high velocity toward the WD surface; and the post-shock flow, where the hot, low-velocity flow settles onto the WD surface — the pre-shock flow is the most likely source of the observed broad components of the X-ray emission lines of EX Hya. This conclusion is supported by the following lines of evidence. First, the large widths of the lines (see Table 1) imply that the radiating plasma is moving with large velocities ($v \gtrsim 2000$ km s^{-1}). Second, ionization parameters ($\xi = L_{\rm X}/nr^2$, where $L_{\rm X}$ is the X-ray luminosity, n is the number density, and r is the distance between the source and target of the photoionizing flux) of a few hundred are required to account for the presence of O VIII, Mg XII, and Si XIV (e.g., Kallman & McCray 1982). Third, the emission measure (EM $= n^2V$, where V is the volume) of the photoionized plasma must be large enough to produce the observed flux. Fourth, Mukai et al. (2003) found that the X-ray spectrum of IPs (other than EX Hya!) can be explained by recombination in the photoionized flow.

The second and third items above exclude the accretion curtains and favor the pre-shock photoionized flow as the source of the broad X-ray emission lines. Consider first the accretion curtains: at an inner disk radius of $10\,R_{\rm WD}$ (e.g., Beuermann et al. 2003), the ionization parameter implies a density of around 3×10^{10} cm^{-3}, which implies a volume of $2 \times 10^5\,R_{\rm WD}^3$ to produce the observed O VIII luminosity, which is hundreds of times the volume available at that distance from the WD. Consider next the pre-shock flow: at a distance $0.1\,R_{\rm WD}$, the ionization parameter implies a density of around 3×10^{14} cm^{-3}, which implies a volume of $0.002\,R_{\rm WD}^3$ to produce the observed O VIII luminosity, which is roughly the size of the accretion shock region.

Given these conclusions, we constructed a model of the X-ray line emission from the photoionized flow above the stand-off shock. We assume a WD of mass $M_{\rm WD} = 0.79\,M_\odot$ (Beuermann & Reinsch 2008), corresponding radius $R_{\rm WD} = 5.9 \times 10^8$ cm, and a luminosity $L_{\rm X} = 2.6 \times 10^{32}$ erg s^{-1} at a distance of 64 pc (Beuermann et al. 2003). These parameters and the size of the accretion spots determine the density at the shock, and this density in turn determines the cooling time and shock height.

We assume a dipole magnetic field, which gives a density $n_{14} = n_0\, r^{-2.5}$, where $n_0 = 10^{14}$ cm^{-3} is the density at the base of the pre-shock flow. With this assumption, the flux of the illuminating radiation and hence the ionization parameter drops rapidly just above the shock on a length scale comparable to the shock size. The atomic physics packages described in Miller et al. (2008) are used to compute the ionization and thermal equilibrium and the attenuation of radiation along and perpendicular to the column axis. Table 2 lists the density (n_{14}), the predicted optical depth for electron scattering ($\tau_{\rm e}$) , the size of the accretion spot ($r_{\rm spot}$), the shock height ($h_{\rm shock}$), and the intensities of the observed broad lines. The corresponding radiative recombination continua (RRCs) should be comparable in strength to the predicted line fluxes, but they will be significantly smeared in wavelength and therefore difficult to detect. The models are quite simple in that they include only one-dimensional radiative transfer and neither time-dependent ionization nor compressional heating of the infalling gas [As an aside, I do not understand why there should be compressional heating of the pre-shock flow. Is this due to the assumed dipole field geometry? If so, OK.][J: I guess so, John?], but they should give roughly the correct intensities for the strong lines. We note that the detection of a broad component in Fe XVII λ16.78, but not λ15.01 supports a photoionization origin (Liedahl et al. 1990), and while the Fe XVII λ16.78 line is weak in the Liedahl et al. model (at densities of 10^{11} cm^{-3}), it is strong at the densities shown in Table 2. It should be noted, however, that the tabulated densities are comparable to the post-shock densities derived by Mauche et al. (2001, 2003)

from the Fe XVII and Fe XXII emission-line ratios, whereas the post-shock density should be higher by a factor of four due to shock compression and by an additional factor due to compression as the shocked gas cools. The latter would be an order of magnitude for a steady flow, but could be much smaller due to the thermal instability of radiative shocks (Chevalier & Imamura 1982).

Table 2. Photoionization model results. Flux in units of 10^{-4} photons cm^{-2} s^{-1}.

Parameter	Model A	Model B	Model C	Model D	Observed Flux[a]
n_{14}[b]	0.41	2.7	12.	30.	···
τ_e	0.03	0.19	0.73	1.8	···
r_{spot}[c]	0.098	0.056	0.031	0.018	···
h_{shock}[d]	0.62	0.19	0.062	0.019	···
d[e]	7	0.5	0.078	0.037	···
O VIII λ18.97	2.34	2.09	2.45	3.08	$2.77^{+0.3}_{-0.3}$
Mg XII λ8.42	0.07	0.08	0.10	0.09	$0.53^{+0.10}_{-0.09}$
Si XIV λ6.18	0.03	0.05	0.08	0.09	$0.84^{+0.03}_{-0.05}$
Fe XVII λ16.78	0.21	0.16	0.17	0.16	$0.55^{+0.19}_{-0.21}$

[a]For ease of comparison with the model predictions, this column reproduces the broad line fluxes listed in Table 1

[b]Density in units of $n_0 = 10^{14}$ cm^{-3}.

[c]Radius of the accretion spot on the surface of the WD in units of white dwarf radius, $R_{WD} = 5.9 \times 10^8$ cm.

[d]Height of the shock above the WD surface in units of white dwarf radius, $R_{WD} = 5.9 \times 10^8$ cm.

[e]enght required to have a volume $V = \pi r^2_{spot} d = EM(OVIII)/n_{14}$, where

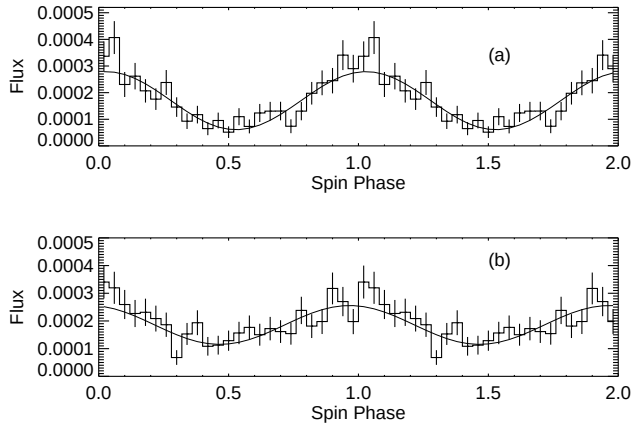

Fig. 2.— Light curves from the blue (a) and (b) red sides of the broad component of O VIII. Error bars are one standard deviation of the count rate in each bin. Solid curve represents the sine wave fit.

$EM(OVIII) = 7 \times 10^{52} cm^{-3}$.

4. Discussion and conclusions

We discuss briefly the implications of the parameters obtained with our photoionization model. First, the height of the shock must be larger than $\approx 0.015\,R_{\rm WD}$ to account for the observed modulation in the X-ray light curves (Allan et al. 1998; Hoogerwerf et al. 2006), but less than $\sim 2\,R_{\rm WD}$ to account for the ~ 20 keV thermal bremsstrahlung temperature (Fujimoto & Ishida 1987; Brunschweiger et al. 2009). Second, the predicted densities cannot be higher than the values derived by Mauche et al. (2001, 2003) from the Fe XVII and Fe XXII emission-line ratios. Table 2 shows that the models predict an O VIII flux that is in good agreement with the observed value, but the predicted Si XIV flux is too small by a factor of 9–30. Given the simplicity of our one-dimensional photoionization model, the agreement of the line fluxes with observations is adequate. The simple model also predicts that the Doppler width ($v \approx 2000$ km s^{-1}) of the ionized material is smaller than the ~ 6000 km s^{-1} free-fall velocity (see § 1). If the column were observed face-on, this large Doppler shift would be seen. The smaller observed line width suggests that the accreting poles remain in the vicinity of the WD limb as seen from Earth, as supported by the small spin-phase radial velocity variations observed by Hoogerwerf et al. (2005).

Models A and B are both acceptable in terms of their agreement with the flux measurements. Also, the predicted height of the shock (0.19–0.62 $R_{\rm WD}$) accounts for the observed modulation of the broad component of O VIII (§3.2) as being caused by phase-dependent absorption. As can be seen in Table 2, the optical depth for electron scattering in Models A and B is low and its contribution to the light curve modulation and absorption is small. This fits in with the observation that the Fe Kα line is quite weak in EX Hya compared with other magnetic CVs (Hellier & Mukai 2004), since little Fe Kα is produced in the accretion flow (although the irradiated WD surface should also produce Fe Kα emission). [I guess that the shock height is not large enough to reduce the solid angle

subtended by the WD and hence reduce the strength of the Fe Kα emission?][[Well, George & Fabian (1991,MNRAS,249,352) computed a EW=100 eV in the case that the reflector subtends a 2π solid angle over the thermal X-ray source (kT=20 keV) and the angle between the observer's line of sight and the normal of the reflecting surface is 60 degrees. Now, I measured EW=36 eV in the chandra data]]. Nonetheless, as show in Table 2, the required length to obtain the observed O VIII emission measure for Model A is $d \sim 7R_{WD}$. As $d > 2R_{WD}$ it implies that most of the emitting volume would not get eclipsed by the body of the WD and therefore we should observe a constant level of emission regardless the spin phase. As this is not the case (see §3.2), we can ruled out model A.[[J: another reason to discard model A is that if d=7R$_{WD}$, it is comparable to d=10 R$_{WD}$ that is the distance of the accretion disk interior edge, then the emitting volume for OVIII would be similar to the whole accretion stream volume, but as John's model imply that the ionization factor drops rapidly with r, we can ruled out this model. Which argument do you prefer?, both?]]

Models C and D have densities higher than those obtained from the Fe XVII and Fe XXII (Mauche et al. 2001, 2003) line ratios. The combination of high densities and small accretion spot size implies significant optical depth for electron scattering (see Table 2), which could help to explain the modulation observed at high energies (*Ginga* data analyzed by Rosen et al. 1991 show a 9–10% pulsed fraction in the 6–8 keV band) but on the other hand it would imply a pulsed fraction on the order of 100% in the soft X-ray band, which is not observed (Rosen 1992). Moreover, Model D implies a small shock height, which would lead us to observe no net modulation in the light curves (Allan et al. 1998), as well as the presence of two spikes, as observed in the light curve of the Mg XI line by Hoogerwerf et al. (2006). None of these effects is observed in the light curves of the broad components of the emission lines (see Fig. 2), therefore we can discard Models C and D.

Summarizing, we detect for the first time in X-rays a broad component in the emission

line profiles of EX Hya and suggest that its origin is related to photoionization of a region in the pre-shock flow by radiation emitted in the collisionally ionized post-shock cooling flow. Such an origin is conforming with the broad emission lines observed in the O VI (Mauche 1999) and C IV (Belle et al. 2003) emission lines in the UV — lines whose widths and flux and radial velocity modulations are consistent with an origin in the pre-shock flow. Although rather simple, our photoionization model constrains the height of the shock and the size of the accretion spot. The height of the shock, from Model B, and the region where the photoionized components are formed, are consistent with its modulation at the spin period. Altogether, our observational findings and the results from our model agree with a scenario where the geometry imposed by the specific accretion rate (§ 1) allows most of the photons from collisional excitation to escape freely, and a small fraction of those photons to photoionize the pre-shock gas. In this regard, the X-ray spectrum from EX Hya manifests both features of the "binomial" distribution found by Mukai et al. (2003).

Support for this work was provided by NASA through *Chandra* awards G07-8026X issued by the *Chandra* X-ray Observatory Center, which is operated by the SAO for and on behalf of NASA under contract NAS8-03060. CWM's contribution to this work was performed under the auspices of the U.S. Department of Energy by Lawrence Livermore National Laboratory under Contract DE-AC52-07NA27344.

Facilities: Chandra

REFERENCES

Aizu, K. 1973, Prog. Theor. Phys., 49, 1184

Allan A., Hellier C., & Beardmore A. P. 1998, MNRAS, 295, 167

Belle, K. E., Howell, S. B., Sion, E. M., Long, K. S., & Szkody, P. 2003, ApJ, 587, 373

Beuermann, K., Harrison, Th. E., McArthur, B. E., Benedict, G. F., & Gänsicke, B. T. 2003, A&A, 412, 821

Beuermann K., & Reinsch K. 2008, A&A, 480, 199

Brunschweiger, J., Greiner, J., Ajello, M., & Osborne, J. 2009, A&A, 496, 121

Chevalier, R. A., & Imamura, J. N. 1982, ApJ, 261, 543

Fujimoto, R. & Ishida, M., 1987, ApJ, 474, 774

Hellier, C., & Mukai, K. 2004, MNRAS, 352, 1037

Hoogerwerf, R., Brickhouse, N. S., & Mauche, C. W. 2005, ApJ, 628, 945

Hoogerwerf, R., Brickhouse, N. S., & Mauche, C. W. 2006, ApJ, 643, L45

Kallman, T. R., & McCray, R. 1982, ApJS, 50, 263

Liedahl, D. A., Kahn, S. M., Osterheld, A. L., & Goldstein, W. H. 1990, ApJ, 350, 37

Mauche, C. W. 1999, ApJ, 520, 822

Mauche, C. W., Brickhouse, N. S., Hoogerwerf, R., Luna, G. J. M., Mukai, K., & Sterken, C. 2009, IBVS, 5876

Mauche, C. W., Liedahl, D. A., & Fournier, K. B. 2001, ApJ, 560, 992

Mauche, C. W., Liedahl, D. A., & Fournier, K. B. 2003, ApJ, 588, L101

Miller, J. M., Raymond, J., Reynolds, C. S., Fabian, A. C., Kallman, T. R., & Homan, J. 2008, ApJ, 680, 1359

Mukai, K., Kinkhabwala, A., Paterson, J. R., Kahn S. M., & Paerels F. 2003, ApJ, 586, L77

Rosen, S. R. 1992, MNRAS, 254, 493

Rosen, S. R., Mason, K. O., & Córdova, F. A. 1988, MNRAS, 231, 549

Rosen, S. R., Mason, K. O., Mukai, K., & Williams, O. R. 1991, MNRAS, 249, 417